INVITED PAPER

Subwavelength-Grating Metamaterial Structures for Silicon Photonic Devices

Building on the improvements in high-resolution lithography for silicon, one can create artificial dielectrics, periodic structures in silicon photonics with periods substantially smaller than a wavelength of light in the material. This paper discusses the theory and applications of these subwavelength structures.

By Robert Halir, Alejandro Ortega-Moñux, Daniel Benedikovic, Goran Z. Mashanovich, J. Gonzalo Wangüemert-Pérez, Jens H. Schmid, Íñigo Molina-Fernández, and Pavel Cheben

ABSTRACT | Segmenting silicon waveguides at the subwavelength scale produce an equivalent homogenous material. The geometry of the waveguide segments provides precise control over modal confinement, effective index, dispersion and birefringence, thereby opening up new approaches to design devices with unprecedented performance. Indeed, with ever-improving lithographic technologies offering sub-100-nm patterning resolution in the silicon photonics platform, many practical devices based on subwavelength structures have been demonstrated in recent years. Subwavelength engineering has thus become an integral design tool in silicon photonics, and both fundamental understanding and novel applications are advancing rapidly. Here, we provide a comprehensive review of the state of the art in this field. We first cover the basics of subwavelength structures, and discuss substrate leakage, fabrication jitter, reduced backscatter, and engineering of material anisotropy. We then review recent applications including broadband waveguide couplers, high-sensitivity evanescent field sensors, low-loss devices for mid-infrared photonics, polarization management structures, spectral filters, and highly efficient fiber-to-chip couplers. We finally discuss the future prospects for subwavelength silicon structures and their impact on advanced device design.

KEYWORDS | Fiber-to-chip coupler; filter; metamaterial; mid-infrared; near-infrared; polarization; silicon photonics; sensor; subwavelength grating; waveguide; waveguide coupler

I. SUBWAVELENGTH STRUCTURES IN SILICON WAVEGUIDES

All-dielectric metamaterials, understood as artificial subwavelength structured materials with optical properties controlled by design, have been the object of intense research for more than a decade [1]–[4]. Among these metamaterials, subwavelength gratings (SWGs) have become an important tool to develop practical, high performance integrated silicon photonics devices, including low-loss fiber-to-chip couplers, highly selective filters, and ultra-broadband waveguide couplers, to name a few. Here, we briefly discuss the fundamentals of this rapidly progressing field and provide an overview of recent applications; for additional details on the theoretical framework and the historic evolution of SWGs in silicon waveguides see [4].

An SWG metamaterial waveguide is a slab structured at a scale smaller than the wavelength of light propagating

Manuscript received November 11, 2017; revised April 9, 2018; accepted June 21, 2018. Date of publication August 3, 2018; date of current version November 20, 2018. This work was supported by the Ministerio de Economía y Competitividad, Programa Estatal de Investigación, Desarrollo e Innovación Orientada a los Retos de la Sociedad (cofinanciado FEDER), Proyecto TEC2016-80718-R, and the Universidad de Málaga. *(Corresponding author: Alejandro Ortega-Moñux.)*

R. Halir, **A. Ortega-Moñux**, **J. G. Wangüemert-Pérez**, and **Í. Molina-Fernández** are with the Departamento de Ingeniería de Comunicaciones, ETSI Telecomunicación, Campus de Teatino, Universidad de Málaga, 29071 Málaga, Spain, and also with Bionand Center for Nanomedicine and Biotechnology, Parque Tecnológico de Andalucía, 29590 Málaga, Spain (e-mail: aom@ic.uma.es).

D. Benedikovic is with the Centre de Nanosciences et de Nanotechnologies, CNRS, Univ. Paris-Sud, University of Paris-Saclay, C2N - Orsay, 91405 Orsay cedex, France (e-mail: daniel.benedikovic@c2n.upsaclay.fr).

G. Z. Mashanovich is with the Optoelectronics Research Centre, University of Southampton, Southampton SO17 1BJ, U.K. (e-mail: g.mashanovich@soton.ac.uk).

J. H. Schmid and **P. Cheben** are with the National Research Council Canada, Ottawa, ON K1A 0R6, Canada (e-mail: pavel.cheben@nrc-cnrc.gc.ca).

Digital Object Identifier 10.1109/JPROC.2018.2851614

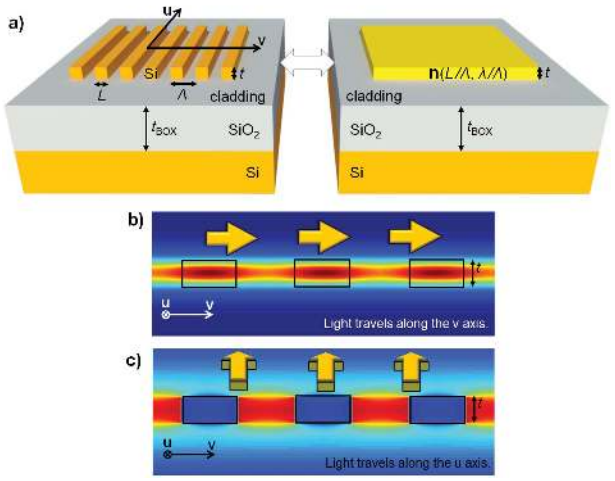

Fig. 1. *(a) An on-chip subwavelength grating metamaterial behaves like a homogeneous slab with a refractive index n, that depends on the polarization of light, the duty cycle of the structure (f = L/Λ), and wavelength-to-period ratio (λ/Λ). The cladding material is not shown for clarity. (b) and (c) Electric field profiles of the in-plane modes travelling in the segmented structure along the v axis (b) and along u axis (c). The t = 220 nm thick silicon segments are shown with black outlines; Λ= 200 nm, f = 50%, λ= 1.55 μm.*

through it, thereby suppressing diffraction effects, and acting as a homogeneous slab waveguide made of an equivalent birefringent material. Fig. 1(a) shows a canonical structure in silicon-on-insulator (SOI), comprising alternating strips of silicon (waveguide core) and the cladding material, as first demonstrated in a silicon wire waveguide by Bock *et al.* [5]. The geometry of the fully etched structure provides lithographic control over the equivalent refractive index, dispersion and material birefringence.

The deep subwavelength regime ($\Lambda \leq 100$ nm for $\lambda \sim 1.55$ μm) is particularly suitable to gain a conceptual understanding of these structures. In this regime, the refractive indexes of the equivalent material for polarization parallel ($n_\parallel$) and perpendicular ($n_\perp$) to the silicon segments can be approximated by Rytov's formulas [6]

$$\begin{aligned} n_\parallel^2 &\approx f n_{\mathrm{Si}}^2 + (1-f) n_{\mathrm{clad}}^2 \\ n_\perp^{-2} &\approx f n_{\mathrm{Si}}^{-2} + (1-f) n_{\mathrm{clad}}^{-2}, \quad \text{for } \Lambda \ll \lambda \end{aligned} \tag{1}$$

where $f = L/\Lambda$ is the duty cycle of the grating structure and n_{Si}, n_{clad} are the refractive indexes of the silicon core and the cladding material, respectively. By varying the duty cycle of the structure, equivalent indexes between those of the silicon core and the cladding material can be engineered, and modal confinement can be controlled. In the deep subwavelength regime, the metamaterial structure does not contribute to dispersion, i.e., the wavelength dependence of the equivalent refractive indexes is determined by the dispersion of the constituent materials. The material birefringence effect becomes relevant when considering light propagating through the SWG structure with its electric field in the plane of the chip [see Fig. 1(a)]. When the propagation is along the **v** axis (electric field parallel to the silicon segments), light experiences a homogeneous slab with refractive index $n_\parallel$, whereas for the propagation along the **u** axis (electric field perpendicular to the silicon segments), light experiences a homogeneous slab with a smaller refractive index $n_\perp$. In analogy to a uniaxial crystal, the equivalent homogenous material can then be described by the refractive index tensor $\mathbf{n} = \mathrm{diag}[n_\parallel, n_\parallel, n_\perp]$ [7].

However, fabricating devices in the deep subwavelength regime is not practical at telecom wavelengths, because even with a 50% duty cycle the required feature sizes of the order of 50 nm are at the limit of e-beam lithography. For larger, and therefore more practical periods (of the order of $\Lambda \sim 300$ nm for $\lambda \sim 1.55$ μm), Rytov's formulas provide an approximate estimate of the equivalent indexes but can no longer be considered accurate. A rigorous description of the structure then requires modal analysis. Propagation along the **v** axis is described in terms of Bloch-Floquet modes [8]; see Fig. 1(b). When the grating period equals one-half of the effective wavelength in the waveguide, the structure exhibits Bragg resonance, or, equivalently, a band-gap, and can thus no longer be described as an equivalent homogenous material. However, for periods just below the Bragg threshold, the structure behaves as a metamaterial with controllable dispersion. Propagation along the **u** axis can be described with waveguide array modes, see Fig. 1(c). Due to the strong field discontinuities at the segment interfaces, the structure is generally dispersive.

A variety of numerical solvers has been developed for these structures (see, for instance [9]and [10]), and both free and commercial solutions are available, including MIT's Photonic-Bands, Rsoft's BandSolve and Photon Design's CrystalWave.

II. ADVANCES IN SWG FUNDAMENTALS

This section is dedicated to some of the fundamental aspects, design advantages and limitations that arise when designing and fabricating waveguide devices with SWG structures. Specifically, we discuss the use of SWG intrinsic anisotropy, the potential for reducing waveguide backscatter, the control of substrate leakage, and the influence of fabrication jitter.

A. Exploiting SWG Anisotropy

In an isotropic medium, the components of the wavevector are related by the expression $k_u^2 + k_v^2 = (nk_0)^2$, where $k_0 = 2\pi/\lambda$. In an SWG, understood as a uniaxial crystal, the dispersion relation becomes [7]:

$$\frac{k_u^2}{n_\perp^2} + \frac{k_v^2}{n_\parallel^2} = k_0^2. \tag{2}$$

The use of such an anisotropic material as waveguide cladding was proposed to enhance modal confinement

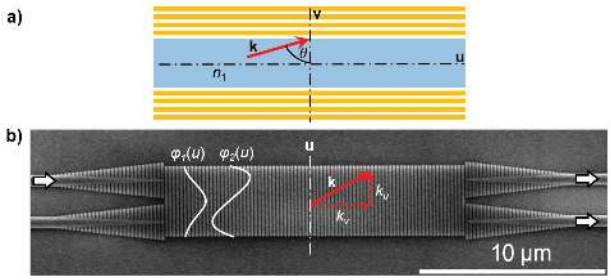

Fig. 2. *(a) When light is incident from a homogenous waveguide core onto a birefringent cladding material, such as an SWG, the conditions for total internal reflection are relaxed, and a stronger light confinement is possible. (b) Scanning electron microscope image of a multimode interference (MMI) beam-splitter with measured bandwidth of more than 300 nm in the telecom 1.55 μm band. The SWG in the central region is anisotropy-engineered to optimize propagation constants of the Bloch-Floquet modes for broadband operation. The four input/output tapered regions provide a smooth transition to the interconnection single mode waveguides.*

in silicon waveguides, see Fig. 2(a) [11]. When a wave polarized within the waveguide plane and with wavevector $\mathbf{k}$ is incident from the isotropic waveguide core onto the anisotropic cladding, the tangential component $k_u = n_1 k_0 \sin(\theta)$, is conserved. From (2) it follows that for angles $\theta \geq \text{asin}(n_\perp / n_1)$ the wave is evanescent in the cladding ($k_v^2 \leq 0$), i.e., it undergoes total internal reflection. The decay rate in the cladding, given by the magnitude of k_v, can be controlled through $n_\parallel$. This effect was recently demonstrated using SWG cladding to reduce cross-talk and bending losses in silicon waveguides [12], [13]. For the wave to penetrate the SWG cladding, small gaps of ~50 nm are required at telecom wavelengths.

On the other hand, the use of an SWG as an anisotropic waveguide core provides unique control over the modal propagation constants [14]. Referring to the central SWG waveguide in Fig. 2(b), for the m-th propagating mode, $\varphi_m(u)$, the transverse wavevector is $k_u \approx m\pi / W$, where W is the waveguide width. From (2) the propagation constant k_v can be found for this mode, that depends on both $n_\parallel$ and $n_\perp$. This effect can be used to engineer the beat length of the first and second mode, enabling multimode interference couplers with unprecedented bandwidths. The 2 × 2 MMI coupler in Fig. 2(b) was experimentally shown to cover the 1.4–1.7 μm band, and bandwidths of more than 500 nm are feasible according to simulations [14]. The minimum feature size is 95 nm for this device. While such dimensions are readily achieved with e-beam lithography and some deep-uv processes [15] completely filling the gaps between the silicon segments with the SiO_2 upper cladding can be challenging. Albeit the small remaining air pockets would not fundamentally change the behavior of the device, they will slightly alter the equivalent refractive index of the subwavelength structure [14], which may need to be included in the simulations.

B. Reducing Backscatter

The modal confinement of an SWG waveguide can be engineered by controlling the duty cycle (f) of the segmented core. Fig. 3(a)–(c) shows the field distribution of the fundamental mode of a typical single-mode SWG waveguide (400 nm × 220 nm) with pitch $\Lambda = 200$ nm and duty cycles $f = 30\%$, 50% and 70%, respectively. By lowering the duty cycle, the equivalent index of the core decreases [see (1)] and the mode is delocalized from the waveguide core [Fig. 3(a)], thereby reducing the interaction with the silicon and its high-index contrast interfaces. IBM researchers have shown that this reduced interaction results in a substantially lower level of backscattering from an SWG waveguide compared to a conventional silicon wire waveguide [16]. The delocalization of the mode is also important for sensing applications (Section III-B) and high efficiency fiber-to-chip couplers (Section III-D).

C. Mitigating Substrate Leakage Loss

Although SWG waveguides are theoretically lossless, their reduced modal confinement, combined with the finite thickness of the buried SiO_2 (BOX) layer [see Fig. 1(a)], may lead to substrate leakage losses. Whereas conventional Si-wires with typical BOX thicknesses t_{BOX} ~2–3 μm exhibit negligible leakage, SWG waveguides with an expanded mode size may have significant losses for the same BOX thicknesses. This fact must be considered at the design stage to mitigate the effects of power leakage in SWG structures. For example, in [16] the modes are weakly confined to the point that the Si handle wafer needs to be undercut to prevent leakage. In [17], the authors demonstrated that there is an exponential relation between the Bloch–Floquet mode effective index

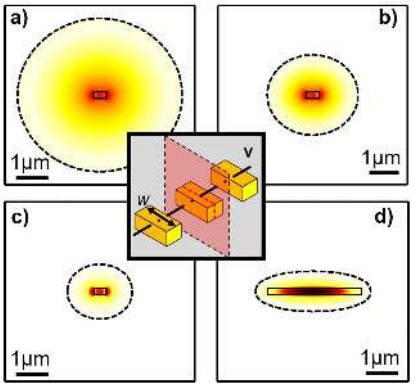

Fig. 3. *Electric field of the fundamental TE Bloch-Floquet mode propagating along the v axis in an SWG waveguide. The fields are shown in the central plane of the Si segment (see the inset). Silicon thickness and grating period are t_{Si}= 220 nm and Λ= 200 nm. Waveguide width and duty cycle are: (a) w = 400 nm, f = 30%, (b) w = 400 nm, f = 50%, (c) w = 400 nm, f = 70%, (d) w = 3 μm, f = 50%. Outside the dotted curves the field amplitudes are below 2% of the maximum value.*

Table 1 Footprint and Performance of SWG-Based Waveguide Couplers (Experimental Results)

Ref.	Type	Footprint	Min. feature	Excess Loss	Imbalance	Bandwidth
[24]	1×2 Inv. Design	2.7×2.7 μm^2	50 nm	0.4 dB	–	60 nm
[25]	1×3 Inv. Design	3.6×3.6 μm^2	120 nm	1 dB	1 dB	30 nm
[20]	2×2 Dir. Coupler	2.5×14 μm^2	80 nm	–	0.7 dB	100 nm
[23]	2×2 Adiabatic	1.1×50 μm^2	100 nm	0.5 dB	0.3 dB	130 nm
[14]	2×2 MMI	3.3×25 μm^2	95 nm	1 dB	1 dB	300 nm

and leakage losses in SWG waveguides. This relation does not depend of the specific waveguide geometry, but only on the BOX thickness and the mode effective index (the latter determines the modal confinement). As a rule of thumb, for a BOX thickness $t_{BOX} = 2\ \mu$m (3 μm) and upper silica cladding, designers should avoid the use of SWG waveguides with a mode effective index below 1.65 (1.55).

D. Controlling Jitter Effects

SWG structures are sensitive to fabrication jitter, i.e., small random errors in the placement of the individual silicon segments. It has been recently shown [18] that a jitter as small as 5 nm in the longitudinal position or size of the Si segments of a comparatively wide (multimode) SWG waveguide may cause a significant reduction in the transmittance (~3 dB loss penalty per 100 μm), degrading the device performance. On the other hand, the effect is practically negligible for narrow (single-mode) SWG waveguides. This dependence with the waveguide width shows that the impact of jitter is directly related to the modal confinement. Indeed, the interaction of the light with the perturbation (i.e. the jitter in the longitudinal Si-cladding interfaces) increases with the waveguide width [Fig. 3(b) and (d)]. The uncontrolled jitter of the fabrication process should be below 5 nm when working with wider (multimode) SWG waveguides.

III. APPLICATIONS OF SUBWAVELENGTH STRUCTURES IN SILICON PHOTONICS

This section provides a review of the state of the art in the application of subwavelength structures to integrated silicon photonic devices. We give insight into the device operation and compare the performance of different solutions. The structures and applications include: waveguide couplers (Section III-A), evanescent field sensors (Section III-B), on-chip polarization management (Section III-C), fiber-to-chip couplers (Section III-D), spectral filters (Section III-E) and devices for the mid-infrared (Section III-F). A brief overview of other emerging applications is given in Section III-G.

A. Waveguide Couplers

Waveguide couplers for splitting and combining different streams of light are fundamental building blocks in planar waveguide circuits. In this section, we compare different SWG waveguide coupler designs and compare their experimental performance (see Table 1).

Directional couplers (DC) have been widely used to implement waveguide couplers with arbitrary splitting ratios. Referring to Fig. 4(a), when light is launched into one of the access waveguides, the even and odd supermodes $\varphi_1(u)$, $\varphi_2(u)$ of the central region are equally excited. As these modes propagate along the structure, they accumulate a phase shift and after a propagation distance equal to half the beat-length $L_\pi = \pi/(k_{v1} - k_{v2})$, 50/50 power splitting is achieved. The beat-length is, however, wavelength dependent, which limits the operational bandwidth of the DC devices. In [19] the use of an SWG structure superimposed on the conventional directional coupler was proposed to engineer the dispersion of the supermodes and flatten the wavelength dependence of the beat-length, thereby extending the bandwidth of the DCs. In [20] the same concept was demonstrated for DCs with power splitting ratios of 50/50, 60/40, 70/30 and 80/20 covering a 100-nm bandwidth near λ =1.55 μm. Fig. 4(b) shows an SEM image of one of the fabricated devices.

Multimode interference couplers are intrinsically broadband devices [21], with their performance essentially governed by the beat length of the two lowest order modes

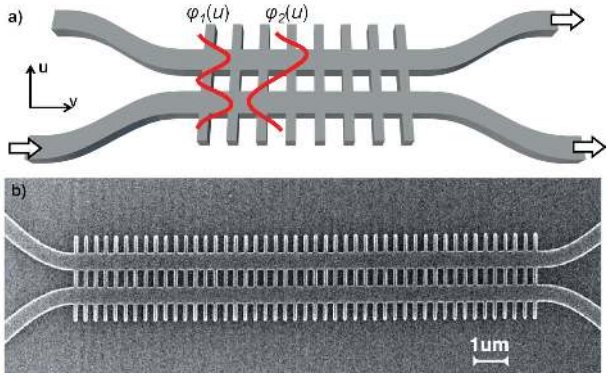

Fig. 4. *(a) Schematic of a broadband SWG enginered DC coupler with virtually constant coupling ratio over a 100-nm bandwidth at telecom wavelengths, as first proposed in [19]. The SWG region between the waveguides is responsible for engineering the dispersion, and SWG regions outside the waveguides suppress the excitation of a spurious higher order mode. (b) Scanning electron image of the experimental demonstration [20]. Reproduced with permission from [20] 2016 IEEE.*

in the multimode region [see Fig. 2(b)]. As discussed in Section II-A, engineering of the anisotropy of the multimode region through SWG structures enables extreme broadband operation, with bandwidths in excess of 300 nm at telecommunication wavelengths [14].

Broadband operation can also be achieved with adiabatic couplers, where the input mode is smoothly converted to the even supermode of two coupled waveguides. While conventional designs require coupling lengths of the order of hundreds of micrometers [22], an SWG-based device as short as 50 μm has been demonstrated [23], with a remarkable performance over a 130-nm bandwidth.

The most compact devices, with footprints of the order of 10 μm^2 have been achieved using "inverse design" approaches, with the local refractive index profile optimized in both the longitudinal and transversal direction to achieve a specific functionality [24], [25]. However, these devices still have a limited performance and smaller bandwidth compared to other solutions.

B. Evanescent Field Sensors

Integrated photonic sensors are typically based on the evanescent field principle. The evanescent tail of a propagating mode interacts with its surroundings to "sense" changes in the superstrate material. This produces a change in the effective index of the propagating mode, which is then transformed into a readily measurable magnitude, e.g., a power variation (in a Mach–Zehnder interferometer) or a resonance wavelength shift [in a ring resonator; see Fig. 5(a)]. Sensing can be based on the change in the effective index produced by a variation in the refractive index of the surrounding material (bulk sensing), or by an increase in the thickness of the adsorbed molecular layer (surface sensing), as schematically shown in Fig. 5(b). The latter, which is typically used for biosensors, requires prior functionalization of the top and sidewall surfaces of the waveguide with selective bioreceptors.

To characterize the performance of the sensors, two figures of merit are typically employed, the sensitivity (S) and the limit of detection (LoD). In ring resonator-based architectures they are respectively defined as: $S_{\text{bulk}} = \Delta\lambda_{\text{resonance}}/\Delta n_{\text{cladding}}$; $S_{\text{surface}} = \Delta\lambda_{\text{resonance}}/\Delta\rho_{\text{adsorbed}}$ and $\text{LoD} = \Delta\lambda_{\text{min,detectable}}/S$.

In order to develop sensors with high sensitivities, waveguides that provide a large overlap of the mode field with the analyte are required. This principle was first realized and used for Si-wire waveguides in [26]. The potential of SWGs as sensing waveguides was first studied in [27]. The authors showed that a sensitivity enhancement can be achieved through the combined delocalization of the mode profile and the additional interaction of analyte with the mode field in the SWG gaps, where a strong longitudinal component of electric field is observed [Fig. 5(a), inset]. Simulation results showed that SWG waveguides operating in TE polarization achieve a six-fold and two-fold sensitivity enhancement compared to TE- and TM-mode sensitivities, respectively, for conventional Si-wire waveguide sensors. It was also shown that the sensitivity does not substantially vary for different silicon waveguide thicknesses.

Since then, several other groups have made important contributions to experimentally demonstrate SWG-based biosensors. In [28] SWG waveguides were used in a ring resonator sensor. The bulk sensitivity of SWG-based rings was estimated as $S_{\text{bulk}} = 383$ nm/RIU (in water). Flueckiger *et al.* reported resonance shifts produced using both salt solutions and bio-molecular binding, obtaining $S_{\text{bulk}} = 490$ nm/RIU (LoD of $2 \cdot 10^{-6}$ RIU) and $S_{\text{surface}} = 0.8$ nm/nm [29], confirming the enhancement factors anticipated in [27]. In [30] a detailed study was carried out to experimentally demonstrate that the surface sensitivity remains constant as the silicon layer thickness increases, which is a unique characteristics of SWG sensing waveguides, predicted theoretically in [27]. The experimental measurements also confirmed the anticipated sensitivity advantage for the SWG-based ring resonator biosensors: 440 nm/RIU and 1 nm/nm for bulk and surface sensing, respectively.

In [31], the authors explore the possibility of using the TM mode in SWG-based racetrack resonators, with some improvements compared to the TE mode. In [32] a sensing architecture is proposed to detect changes both in the real and the imaginary part of the refractive index of the surrounding medium. The SWG bus waveguide of the ring resonator is designed to work as a partially reflecting element at its two ending ports. When such waveguide couples with a cavity, like the ring resonator, a Fabry-Pérot effect is observed and a sharp asymmetric Fano resonance is obtained in the output spectrum. Measuring both the resonant wavelength shift and the reduction in the slope of

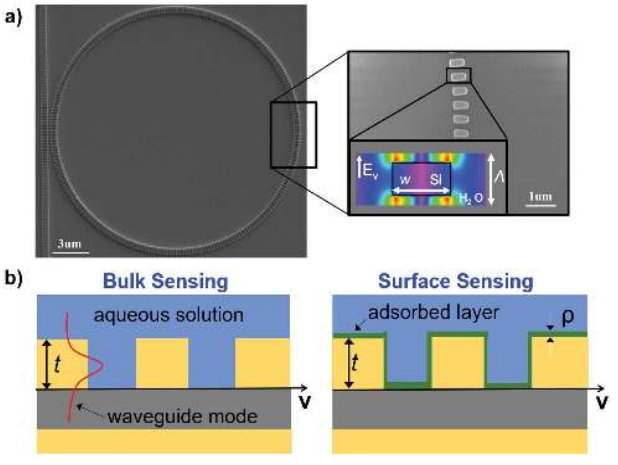

Fig. 5. *(a) SEM image of an SWG ring resonator sensor. Waveguide geometry: w = 500 nm, Λ = 250 nm, t = 220 nm, f = 70%. Adapted with permission from [29]. Inset shows the enhanced longitudinal component of the electric field in the gap between the silicon segments, enhancing the mode interaction with the analyte. (b) Schematics of bulk and surface sensing in SWG waveguides.*

Table 2 SWG-Based Polarization Management Devices at Telecom Wavelengths ($\lambda \sim 1.55\ \mu$ m)

Ref.	Device	Platform	Fab.	Length	Operating Principle	Max.IL @ Bandwidth	Min. ER @Bandwidth	Fabrication Tolerance
[33]	PSR	H= 220 nm	No	40 μm	Asymmetric-DC[b]	0.4 dB @40 nm	10 dB @60 nm	ΔW = ± 40 nm SWG based enhancement
[36]	PSR	H= 220 nm MFS[a] = 60 nm	Yes	35 μm	Asymmetric-DC[b] (based on [33])	1 dB @50 nm	10 dB @85 nm	Careful design of tolerance to several parameters
[37]	PSR	H= 220 nm MFS[a] = 150 nm	Yes	45 μm	Asymmetric-DC[b] (based on [33])	1.5 dB @40 nm	13 dB @40 nm	ΔW = ± 50 nm SWG based enhancement
[38]	PBS	H= 340 nm MFS[a] = 100 nm	No	21 μm	Symmetric-DC[b]	1.5 dB @115 nm	10 dB @115 nm	ΔW = ± 30 nm
[39]	PBS	H= 250 nm MFS[a] = 100 nm	No	6.8 μm	Mode evolution	0.71 dB @115 nm	18 dB @81 nm	ΔW = ± 50 nm for ER > 18 dB
[43]	PF	H= 250 nm MFS[a] =150 nm	Yes	60 μm	TE-pass polarizer (TM mode is leaked)	0.4 dB @110 nm	30 dB @110 nm	Tolerant to duty cycle deviations
[44]	PBS	H= 220 nm MFS[a] =150 nm	Yes	23 μm	Bent DC[b] with SWG based polarization filter	1 dB @60 nm	20 dB @60 nm	—
[40]	PSR	H_1= 250 nm H_2=410 nm	No	8.2 μm	Mode evolution (based on [39])	0.9 dB @200 nm	15 dB @200 nm	ΔW = ± 100 nm for ER > 15 dB

[a]MFS = Minimum Feature Size; [b]DC = Directional Coupler;

Fano resonance, the real and imaginary parts of refractive index are determined.

C. Polarization Management

Polarization control is becoming increasingly important in silicon photonics circuits for telecom and datacom applications. On-chip polarization control has been pursued for many years and is still an active field of research, as many of the designs that can be found in the literature exhibit low fabrication tolerances. The design of high performance polarization management devices is challenging because tight constraints must be simultaneously fulfilled for both polarizations, by tuning a rather limited set of parameters. Introducing SWG structures provides the designer with an additional degree of freedom, allowing a more flexible manipulation of birefringence and dispersion. This in turn helps relax design tradeoffs and often results in improved performance and reduced device size. Typical building blocks for polarization control include polarization beam splitters (PBS), polarization rotators (PR), and polarization filters (PF) (polarizers). For the standard silicon thickness of 220 nm, the TM mode is less strongly guided than TE, so it is more convenient to make use of a PBS that not only separates both polarizations, but also rotates the polarization state from TM to TE. Such a device is commonly referred to as a polarization beam splitter and rotator (PSR). Recently, several SWG-based designs for on-chip polarization management have been reported; their performances are summarized in Table 2.

One particularly promising polarization management device based on SWGs is a PSR proposed by Xiong et al. [33]. Fig. 6(a) illustrates the operation principle of the device: while the input TE mode remains in the homogenous (through) waveguide, the input TM mode is phase matched to the fundamental TE mode of the SWG waveguide and couples to the cross output. The cross-coupling between the two polarizations is facilitated by two hybrid supermodes supported in the coupling region; the asymmetries of the vertical and horizontal components of their electric fields are created not only by the geometry of the directional coupler, but also by the vertical asymmetry arising from different refractive indexes of the upper and bottom cladding media [34], [35]. The device builds upon a previously proposed asymmetric directional coupler [34], but improving its performance by using SWG engineering, specifically to increase the tolerance to waveguide width errors by a factor of 10. Fabrication and characterization of this type of PSR was carried out in [36] and [37]. In [36] the device was optimized with some improvements in bandwidth and size, and measurements showed only a slight deterioration of expected insertion losses (IL). It was also shown that if fabrication deviations affect not only the transverse dimensions (waveguide width and the gap) but also the length of silicon blocks and consequently the SWG duty cycle, this PBS would be less fabrication tolerant, but still twice as tolerant as a conventional device. In [37] an additional TM filter was included at the TE output port to increase the PSR extinction ratio (ER). Fig. 6(b) shows an SEM picture of the fabricated device.

SWGs have also been used in [38] and [39] to improve the performance of polarization beam splitters. In [38] the authors reported an SWG assisted directional coupler in a nonstandard 340-nm SOI platform, using the concept of the colorless directional coupler in [19] in which the SWG medium is engineered to match the beat-lengths for TE and TM polarizations ($L_{\pi,\mathrm{TM}} = 2L_{\pi,\mathrm{TE}}$). In [39] a very compact PBS based on mode evolution was presented, with promising simulation results. In a further refinement [40], the same authors proposed a compact PSR based on a similar approach. The device is remarkable as it combines the splitting and rotation functionality in a compact design with a very good optical performance. However, its practical implementation is more complicated because it relies on a nonstandard 410-nm silicon thickness, requires two etch steps (full 410- and 160-nm etch depths), and output ports require waveguides of different thickness.

Other SWG engineered PBS and PR have been reported, [41], [42], based on horizontal slot waveguides and cross slot waveguides.

Finally, SWGs have also been explored to improve the performance of polarizers. In [43] the authors use SWG engineering to make a nonreflective polarizer: the waveguide width and effective index are simultaneously designed to adjust the TM mode cutoff condition of the waveguide without perturbing the TE mode. The TM mode is leaked to the substrate, with a high extinction ratio (ER). Furthermore, an SWG-based TM-pass polarization filter was used in [44] to increase the ER of a bent DC-based PBS.

Subwavelength structures have also been successfully used to design polarization management devices in SOI by means of optimization algorithms. In [45] a $2.4 \times 2.4\ \mu m^2$ footprint PBS was designed by means of a nonlinear optimization algorithm in a single etch step 300 nm SOI platform, experimentally achieving ER >10 dB in a moderate 32 nm bandwidth. More recently, the same group [46] reported a PR based on the same approach, with some experimental results. An improved performance was achieved in [47] for a metamaterial PR designed by a genetic algorithm. The device fabricated in a two etch step 220 nm SOI exhibited an ER >10 dB and 140 nm bandwidth.

D. Low-Loss Fiber-to-Chip Couplers

Practical deployment of nanophotonic technologies requires the availability of efficient input/output optical interfaces. Coupling of light to or from planar waveguide circuits has been recognized as a major practical challenge since the early years of integrated optics. Two coupling solutions are typically used, surface grating couplers [4], [48]–[71] and edge couplers [1], [72]–[78]; for a comprehensive review of this field see the paper by Vermeulen in this special issue. In the following we focus on the use of SWG structured metamaterials to enhance performance in fiber-chip coupling [1], [49]–[56], [59]–[63], [65]–[67], [69]–[77].

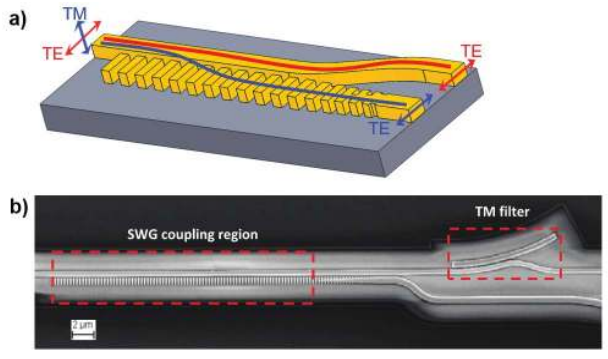

Fig. 6. *(a) Schematic structure of the SWG-PSR with enhanced fabrication tolerance proposed in [33]. (Adapted with permission from [33].) (b) SEM image of the experimental demonstration [37]; a bent DC is included at the TE output port to ensure a high ER for the TM-polarized light input. (Reproduced with permission from [37].)*

1) Surface Grating Couplers: Surface grating couplers (GCs) use a diffraction grating to resonantly couple the light between planar waveguides and optical fibers, see Fig. 7(a). GCs are particularly interesting as they allow wafer-scale testing and relaxed alignment tolerances for fiber attachment. Recently, several implementations of GCs were reported [54]–[64], with the grating directionality being the key parameter to reach high coupling efficiency. Benedikovic *et al.* showed that high-efficiency single-etch GCs can be realized for a given BOX thickness, by exploiting an interference effect [54]–[56]. By adjustment of the radiation angle, the light reflected at the BOX-substrate interface interferes constructively with the light diffracted upwards (towards the optical fiber), increasing coupler directionality. Coupling efficiency of -2.2 dB at 1.55 μm [54], [55] and -2.5 dB at 1.31 μm wavelengths were demonstrated experimentally in a standard 220-nm SOI platform [56]. Furthermore, by using backside metallization, a record subdecibel efficiency of -0.69 dB was demonstrated for a single-etch step SWG-engineered surface grating coupler (220-nm SOI) [55]. An alternative way to achieve high-efficiency GCs is to increase the intrinsic directionality of the grating. This can be realized by using the blazing effect [57]–[63]. The latter can be achieved with interleaved grating arrangements [57]–[60] or employing an L-shaped grating teeth geometry [62], [63]. Blazed GCs typically have excellent directionality ($>95\%$), independently on the BOX thickness, thereby favoring implementation on various photonic platforms [57]–[63]. An interleaved GC that includes a short SWG-index matching section to reduce reflectivity at the waveguide-grating junction was reported in [59] and [60].

Experimentally, an efficiency of -1.3 dB was achieved at 1.55 μm in 220 nm SOI. Recently, Chen *et al.* employed a continuous SWG metamaterial apodization in an interleaved GC, predicting a subdecibel efficiency of -0.7 dB, with the measured coupling loss -1.9 dB near 1.31 μm [61]. The L-shaped GC with perfectly vertical light emission was demonstrated by Watanabe *et al.* [62] on 220 nm SOI platform, with a longitudinal pattern of SWG pillars to suppress reflectivity ($\sim 1\%$, theory). The couplers were fabricated by e-beam lithography, with a measured efficiency of -2.6 dB. L-shaped GC fabricated by 193 nm deep-UV lithography using 300-nm-thick Si layer on 300-mm SOI wafers has been reported in [63]. A transversal SWG nanostructure was included as a short anti-reflection region at the interface between the access waveguide and the grating region. The tested devices have an efficiency of -2.7 dB, with eight-fold reduction of back-reflections, to $\sim 1\%$. Recently, Zhu *et al.* reported a GC design with high-index-contrast metastructure (HICM) [64]. Here, the resonant behavior of HICM was used to improve the coupling of out-of-plane waves

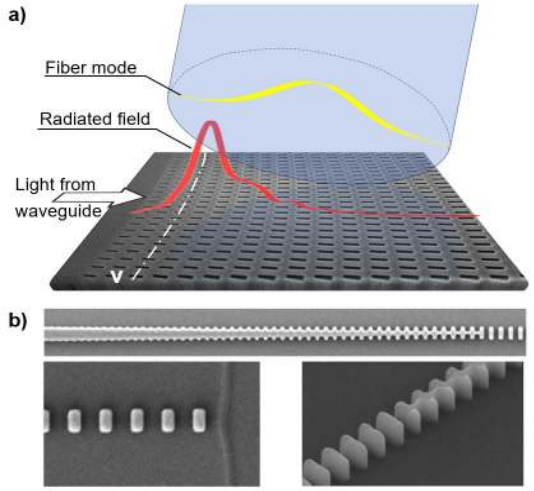

Fig. 7. *Fiber-chip coupling techniques: (a) A fiber-to-chip grating coupler diffracts power from a silicon waveguide towards an optical fiber. The subwavelength structure (along the v direction) provides control over the properties of the radiated field. (b) In a subwavelength engineered inverse taper, polarization independent operation can be achieved. (Reproduced with permission from [74].)*

into an in-plane waveguide, with an efficiency of −0.32 dB and a bandwidth of 48 nm. It was suggested that this concept can be useful for compact spectral multiplexers with high efficiency and broadband wavelength response [64].

Conventional GCs for SOI waveguides typically exhibit a limited 1-dB bandwidth of 30-40 nm. This is a direct consequence of the wavelength dependence of the grating radiation angle [4]. Recently, several interesting wideband designs were proposed [65]–[68]. Zhong *et al.* showed a focusing GC with dispersion-engineered SWG structure, with an efficiency of −4.7 dB and a 1-dB bandwidth of ∼100 nm [65]. Wang *et al.* reported a single-etch SWG-assisted 1-D grating, with a measured efficiency of −3.8 dB and flatband operation up to 90 nm [66]. Sánchez-Postigo *et al.* [67] proposed a promising device concept for highly efficient and ultra-broadband operation, using the zeroth diffraction order. The coupler operates fully in the SWG regime, with an index-engineered SWG waveguide core, which results in a dramatically broadened bandwidth. The SWG grating is assisted by a silicon prism. As a result, the coupling efficiency and the spectral bandwidth are optimized simultaneously. An apodized design yields an unprecedented efficiency-bandwidth product, with a coupling efficiency of −0.41 dB and a 1-dB bandwidth of 126 nm [67]. Passoni *et al.* [68] showed by theoretical analysis that optical fibers with smaller mode field diameters (MFDs) can be used for enlarging the spectral bandwidth of GCs towards 100 nm.

The GCs may also serve as polarization selective devices. The effective Bloch-Floquet mode index in the grating region exhibits a large birefringence, resulting in different coupling angles for TE and TM polarizations. This imposes restrictions for applications with incoming light of unknown polarization [4]. Zou *et al.* reported single-etch 2-D GCs with SWG cylinders [69], with a measured efficiency of −6 dB. Further improvement was achieved by using five SWG-structured cylinders of carefully optimized separation, yielding a polarization dependent loss (PDL) as low as 0.25 dB within the C-band [70]. SWG structures can also be advantageously used for grating couplers for mid-IR wavelengths as described in Section III-F.

2) Edge Couplers: Fiber-chip edge couplers can provide high coupling efficiency (>90%) and are suitable for broadband applications. SWG metamaterial couplers, first demonstrated by Cheben *et al.* [1], [73], [74], are becoming the state-of-the-art solution for silicon photonics fiber-chip edge coupling. In the SWG coupler concept [1], [73], the mode size is transformed to match the optical fiber mode by varying the duty cycle of the subwavelength grating formed in the metamaterial waveguide core, see Fig. 7(b). Loss and wavelength resonances are suppressed due to subwavelength nature of the nanostructure, and the mode size is directly controlled by the volume fractions of the core (Si) and cladding (SiO_2 materials, which are defined in a single lithographic patterning step. An SWG metamaterial edge coupler with a coupling loss of −0.32 dB (92% efficiency) and negligible polarization dependence for the telecom wavelength band centered at 1.55 μm has been demonstrated [74]. Barwicz *et al.* at IBM showed a conceptually similar SWG metamaterial coupler, yet optimized to interface cleaved SMF-28 fibers, for the O-, S-, and C- communication bands [72], [75], [76]. To facilitate sufficient mode expansion beyond typically used SOI wafers with 2 μm or 3 μm BOX, local substrate removal was used near the chip facet. The undercut is filled with index-matching adhesive, resulting in negligible leakage penalty to the Si substrate. Devices were fabricated using 193 nm deep-UV optical lithography in a CMOS production facility, with efficiency in a range of −1.6 dB to −0.9 dB, low polarization dependence and wideband coupling performance. Alternatively, Papes *et al.* proposed an edge coupler concept with large mode size [77] that does not require local substrate removal. A few thin high-index Si_3N_4 layers are imbedded in SiO_2 upper cladding to effectively pull the mode upwards, therefore reducing leakage through the buried oxide layer to the Si substrate. The Si_3N_4 layers are gradually tapered out along the coupler by SWG refractive index engineering. The coupling efficiency of −0.42 dB was estimated for TE-polarization at 1.55 μm, with a bandwidth exceeding 100 nm. A similar concept was reported by Picard *et al.*, using a high-index Si_3N_4 multi-rod structure, for polarization-independent coupling with a high-numerical-aperture fiber [78].

E. Spectral Filtering Devices

Spectral filtering is an important functionality in integrated optics, with different applications in the fields of optical communications, biosensing, microwave photonics and quantum optics, among others. Different

filtering schemes have been implemented on the SOI platform, including microring resonators, Bragg gratings and grating-assisted contra-directional couplers. Subwavelength grating structures have been successfully used to improve filter performance such as quality factor and extinction ratio, or to ease the fabrication requirements.

Ring resonators based on SWG waveguides with trapezoidal silicon pillars have achieved high quality factors (Q) and compact footprints [79] (see also Section III-G). However, ring resonators have a limited free spectral range (FSR) and do not have flat-top response for a simple configuration. For these reasons, Bragg gratings and contra-directional couplers are often preferred. In SOI technology the high index contrast makes it difficult to obtain the weak grating coupling coefficients required for high-Q (narrow bandwidth) Bragg gratings. Different configurations of Bragg gratings filters based on SWG structures have been proposed to solve this problem. In [80] the authors demonstrated a Bragg grating comprising two interleaved segmented SWG waveguides with slightly different duty cycles, obtaining a measured 3 dB bandwidth of ∼0.5 nm and a rejection ratio of ∼12 dB. These results were subsequently improved using a similar approach, but based on two interleaved SWG corrugated waveguides with slightly different corrugations widths, instead of a fully segmented core with two different duty cycles [81]. Experimental results demonstrate a rejection bandwidth of ∼1.1 nm with an extinction ratio of more than 40 dB. Finally, numerical calculations reveal that integrated Bragg gratings with subnanometer rejection bandwidths can be designed using a conventional SWG waveguide loaded with lateral silicon segments [82], as shown schematically in Fig. 8(a). The simulated spectral reflectance for weakly coupled loading segments is shown in Fig. 8(b). This device exhibits a very narrow rejection bandwidth of ∼50 pm. Minimum feature size is 100 nm, for compatibility with deep-UV optical lithography.

A drawback of Bragg filters is that, because they operate in reflection, they usually require the use of an off-chip optical circulator or integration in a Mach-Zehnder interferometer [83]. Grating assisted contra-directional couplers have been proposed as an alternative to Bragg filters, especially for applications that require rejection bandwidths larger than 1 nm. Contra-DC filters are based on two strongly asymmetric coupled waveguides with a periodic perturbation that allows for the contra-directional coupling between the two waveguides. SWG waveguides are well suited for this purpose, because a directional coupler combing a conventional photonic-wire waveguide and a SWG waveguide exhibits the high level of asymmetry needed to prevent the undesired co-directional coupling ($k_{PW} \gg k_{SWG}$). Additionally, the SWG provides the periodic perturbation required to achieve contra-directional coupling ($k_{PW} + k_{SWG} = 2\pi/\Lambda$) [84]. Experimental results show that controlling the gap distance between the waveguides, 3 dB bandwidths between ∼20 nm and ∼1 nm can be obtained. The characteristic sidelobes of the wavelength response can be suppressed by apodizing the gap between the waveguides [85]. With this approach, a high sidelobe suppression of ∼27 dB is achieved, at the cost of relatively high insertion losses (∼2.5 dB) and a rather small rejection ratio of the through port (∼5 dB). A detailed study of the compromise between sidelobe suppression and extinction ratio is provided in [86], including practical considerations for the design of add/drop multiplexers based on SWG contra-directional filters. In the same work, the authors propose the introduction of a π phase shift in the middle of the SWG structure to achieve a narrow transmission peak (∼1 nm) within the stop-band of the device. This structure has a potential application in sensing, since the central wavelength of the resonance peak is sensitive to the cladding refractive index, with a simulated bulk sensitivity of 177 nm/RIU.

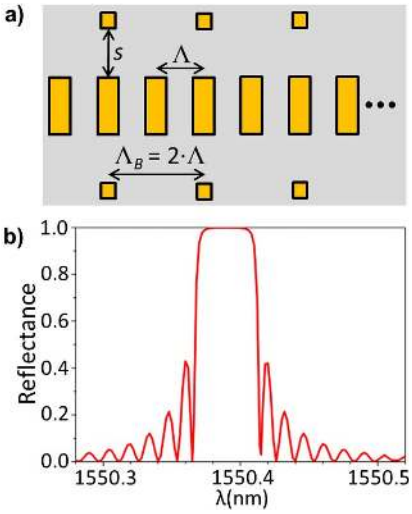

Fig. 8. *Schematics of a Bragg grating in a SWG waveguide with loading segments, as proposed in [82]. (b) Simulated spectral reflectance for a 400-nm-wide SWG waveguide (Λ= 242 nm, DC =60%). The separation between the SWG waveguide and 130 × 130 nm^2 Bragg loading segments is s = 1 μm and the grating length is ∼ 32 mm.*

Filters that separate the 1.3- and 1.55-μm transmission windows, i.e., diplexers, have also been proposed based on SWG structures. In [87] a 2.8 × 2.8 μm^2 footprint diplexer designed with an optimization algorithm was demonstrated, with insertion losses of 2 dB and a crosstalk better than 11 dB over a 100-nm bandwidth. In [88] a diplexer based on a slotted multimode interference coupler [89] was proposed with a length of 43 μm and simulated insertion losses below 1 dB in a 120-nm bandwidth.

F. Devices for the Mid-Infrared

Silicon is transparent up to a wavelength of ∼8 μm, and it is therefore potentially useful for mid-infrared (mid-IR) applications; see the paper by Fedeli and Nicoletti in this special issue for a review on mid-IR silicon photonics. However, the silicon dioxide BOX layer [see Fig. 1(a)]

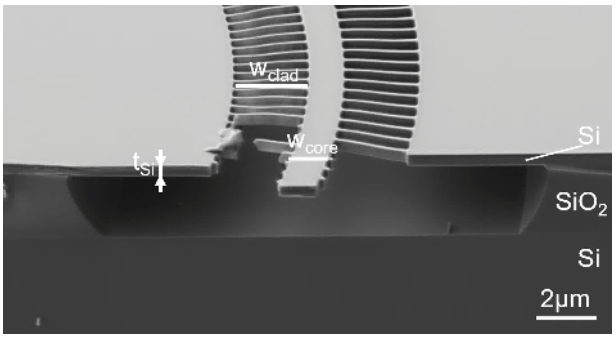

Fig. 9. *A suspended silicon membrane waveguide supported by an SWG cladding strips; the BOX is etched away by hydrofluoric acid that penetrates through the subwavelength holes (the damaged strips are due to the cleaving process) [90].*

is lossy beyond $\lambda \sim 3.6\ \mu$m, which means that the SOI platform cannot be used in most of the mid-IR wavelength range. However, if the buried oxide layer is removed and a suspended Si waveguide formed, the complete transparency range of Si becomes accessible. Subwavelength gratings can be implemented for this purpose and they are particularly suitable for the mid-IR due to their larger feature sizes compared to the near-IR designs. In [90] a suspended mid-IR Si platform has been demonstrated by using SWGs as a lateral cladding and as access points for removal of the BOX layer by etching with hydrofluoric (HF) acid (Fig. 9). The fabrication of these structures involves e-beam lithography, inductively coupled plasma dry etching of the silicon layer, and HF wet etching of the SiO_2 layer. The structure offers better mechanical stability and simpler fabrication compared to rib suspended Si waveguides as the slab is thicker and there is only one dry etch step.

The design of these structures involves a tradeoff between minimizing loss, achieving mechanical robustness, and fabricability of the structures. Minimizing losses requires increasing the waveguide core width (w_{core}) to reduce sidewall scattering, increasing the cladding width (w_{clad}) and decreasing the duty cycle of the SWG to avoid lateral leakage to the silicon slab. Mechanical stability is achieved with a narrow (i.e., lighter) waveguide core, and a narrow cladding region with a larger duty cycle. Finally, the holes in the SWG should be as large as possible to facilitate the HF acid flow.

For the wavelength range of 3.7–3.8 μm and based on $t_{Si} = 500$ nm SOI with $t_{BOX} = 3\ \mu$m, near optimum waveguide dimensions have been found to be $w_{core} = 1.3\ \mu$m, $w_{clad} = 2.5\ \mu$m, subwavelength grating period $\Lambda = 550$ nm, and a duty cycle $f \sim 20\%$ [90]. Based on these dimensions, S- and 90°-bends, multimode interference couplers and Mach–Zehnder interferometers were reported. The demonstrated waveguide propagation loss was as low as 0.8 dB/cm, while S-bend and 90°-bend losses were negligible, whilst Mach-Zehnder interferometers had 15-dB extinction ratio and MMI insertion loss was 0.5 dB. These results pave the way for the realization of a suspended Si platform for longer wavelengths. A suspended silicon waveguides operating at a wavelength of 7.67 μm with a propagation loss of 3.1 ± 0.3 dB/cm has been recently reported [91].

Following this design strategy, Zhou *et al*. demonstrated millimeter-scale-long Si slot suspended waveguides at a wavelength of 2.25 μm [92]. The Si thickness was $t_{si} = 340$ nm, waveguide width $w_{core} = 780$ nm, and slot width 85 nm. The authors used the same period of the SWGs and the width of silicon supports as in [90], with measured propagation loss of 7.9 dB/cm. A fully suspended MIR racetrack resonator with SWG cladding that exhibits loaded Q factors up to 16 440 at $\lambda \sim 2.4\ \mu$m was recently presented in [93].

Due to its high material loss at longer wavelengths, silicon cannot be used in the so-called fingerprint region ($8\ \mu\text{m} < \lambda < 14\ \mu$m). On the other hand, germanium is transparent in this region. An interesting solution is to start with germanium-on-insulator (GOI) platform and suspend Ge. This way, a wideband mid-IR platform ($2\ \mu\text{m} < \lambda < 14\ \mu$m) can be realized. Kang *et al.* reported a focusing SWG coupler [Fig. 10(a)] with a coupling efficiency of −11 dB and a 1 dB bandwidth of 58 nm for coupling TM polarized light into a suspended Ge rib waveguide [Fig. 10(b) and (c)] at a wavelength of 2.37 μm [71]. The GOI was fabricated by wafer bonding using Al_2O_3 layer.

G. Other Applications

Several other examples for the application of subwavelength structures in silicon waveguides have been described in the literature over the past few years. Xiao and Xu demonstrated a subwavelength multi-mode converter for coupling light from a strip to a slot waveguide [94]. In this structure the use of the subwavelength grating reduces the device footprint by a factor of two compared to a conventional coupler based on the same principle and leads to a wide operating bandwidth, two advantageous

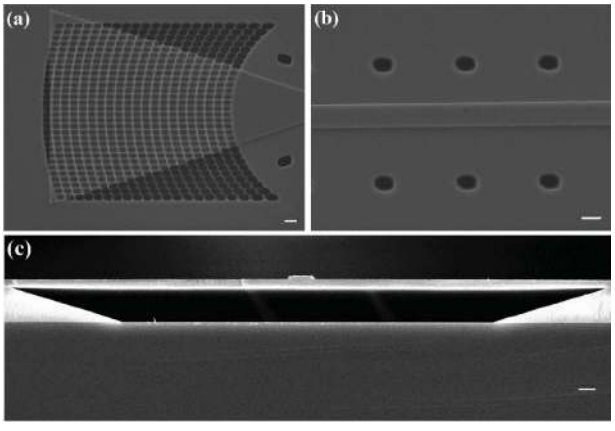

Fig. 10. *SEM images of (a) focusing SWG, (b) suspended Ge rib waveguide, and (c) cross section of the suspended Ge waveguide and substrate. (Reproduced with permission from [71].)*

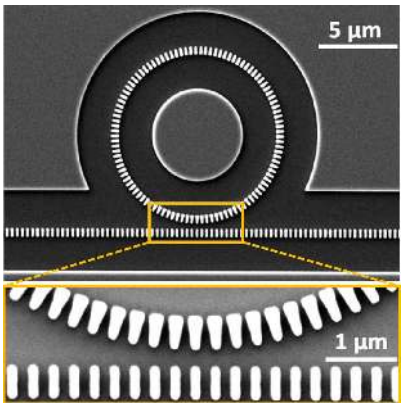

Fig. 11 *SWG waveguide ring resonator with trapezoidal segments to reduce bend losses. (Reproduced with permission from [79].)*

effects that have also been exploited in SWG MMI couplers [14]. A compact optical true time delay line with an array of SWG waveguides of equal length but varying duty cycles has been demonstrated in [95], employing a concept that has previously been used to avoid waveguide bends and minimize device footprint of an on-chip Fourier-transform spectrometer [96]. The reduced interaction of the waveguide mode with the silicon core (see Section II-B) also decreases nonlinearities: in [97] slotted SWG waveguides are shown to exhibit an ultra-low nonlinearity of $3.2\text{W}^{-1}\text{m}^{-1}$, making it possible to transmit signals with higher power through SWG waveguides. In [98] the signal transmitted through a SWG waveguide could be increased by 8 dB compared to a wire waveguide, allowing the transmission of a 75-channel wavelength-division multiplexed (WDM) signal with a data rate of 2.86 Tb/s through a 2-mm-long SWG waveguide. On the other hand, mode delocalization in SWG waveguides makes it difficult to design tight waveguide bends with low radiation losses. In particular, micro-ring resonators made from SWG waveguides are attractive devices for studying light matter interactions but suffer from large bend losses when miniaturized. An innovative solution to this problem has been found by Wang *et al.* [79], who demonstrate increases of the ring resonator Q-factor from 2800 to 11 500 and from 15 000 to 45 000 for bend radii of 5 μm and 10 μm, respectively, by employing trapezoidal SWG elements for the curved waveguides instead of the conventionally used rectangular ones, as shown in Fig. 11.

These trapezoidal SWG elements here implement a simple type of transformation optics, but without requiring grey scale lithography [99]. Another interesting use of an SWG structure as a thermally conductive lateral waveguide cladding is described by Zhang and He [100]. Here, a high-Q silicon nanobeam cavity is thermally tuned by connecting it laterally to a heated silicon slab area via an SWG nanotentacle structure which provides efficient heat transfer and low optical losses. This structure is shown to be more thermally efficient than the conventional heater-on-cladding configuration and can also be used in situations where no upper cladding can be deposited on the waveguide, such as in sensing applications.

The use of SWG waveguides for dispersion engineering is numerically investigated in two papers by Jafaria and Zarifkar [101], [102]. In their study they show a single-etch sidewall SWG waveguide design with a flat dispersion profile over a 1615-nm wavelength range. Flexible and broadband control of SWG waveguide dispersion profiles which include large normal to low anomalous operation regimes is numerically demonstrated by Benedikovic *et al.* [103]. Finally, compact and broadband mode (de) multiplexers based on SWG waveguides have been recently proposed in [104] and [105].

IV. CONCLUSION

Subwavelength grating metamaterials waveguide structures have become a key enabler for high performance silicon photonic devices. Leveraging the available ~100-nm lithographic resolution, they open up the possibility to locally engineer refractive index, dispersion and anisotropy, providing the device designer with new degrees of freedom. As we have shown throughout this review, this has resulted in many high performance devices, ranging from ultra-broadband couplers, high Q-factor filters and efficient fiber-chip couplers, to devices for polarization management, sensing and the mid-infrared applications, among others. Research on integrated subwavelength structures continues at an accelerating pace, with a vast design space remaining to be explored, for example in dispersion and anisotropy engineering. On the other hand, the minimum feature sizes are well within the reach of modern immersion lithography processes, therefore enabling mass fabrication of subwavelength engineered devices and paving the way for their commercial exploitations. ■

REFERENCES

[1] P. Cheben, "Refractive index engineering with subwavelength gratings for efficient microphotonic couplers and planar waveguide multiplexers," *Opt. Lett.*, vol. 35, no. 15, pp. 2526–2528, 2010.

[2] I. Staude and J. Schilling, "Metamaterial-inspired silicon nanophotonics," *Nature Photon.*, vol. 11, no. 5, pp. 274–284, 2017.

[3] P. Cheben, I. Molina-Fernández, D. Smith, W. Zhou, and P. Berini, "Subwavelength photonics," *Opt. Photon. News*, vol. 28, no. 5, pp. 34–41, 2017.

[4] R. Halir, "Waveguide sub-wavelength structures: A review of principles and applications," *Laser Photon. Rev.*, vol. 9, no. 1, pp. 25–49, Sep. 2014.

[5] P. J. Bock, "Subwavelength grating periodic structures in silicon-on-insulator: A new type of microphotonic waveguide," *Opt. Express*, vol. 18, no. 19, pp. 20251–20262, 2010.

[6] S. M. Rytov, "Electromagnetic properties of a finely stratified medium," *Sov. Phys. JETP*, vol. 2, no. 3, pp. 466–475, 1956.

[7] B. E. A. Saleh and M. C. Teich, "Polarization and crystal optics," in *Fundamentals of Photonics*, J. W. Goodman, Ed. Hoboken, NJ, USA: Wiley, 1991, pp. 193–237.

[8] J. D. Joannopoulos, S. G. Johnson, J. N. Winn, and R. D. Meade, "Symmetries and solid-state electromagnetism," in *Photonic Crystals*, 2nd ed. Princeton, NJ, USA: Princeton Univ. Press, 2008, pp. 25–43.

[9] G. Lecamp, J. P. Hugonin, and P. Lalanne, "Theoretical and computational concepts for periodic optical waveguides," *Opt. Express*, vol. 15, no. 18, pp. 11042–11060, 2007.

[10] J. Čtyroký, "3-D bidirectional propagation

algorithm based on Fourier series," *J. Lightw. Technol.*, vol. 30, no. 23, pp. 3699–3708, Dec. 1, 2012.

[11] S. Jahani and Z. Jacob, "Transparent subdiffraction optics: Nanoscale light confinement without metal," *Optica*, vol. 1, no. 2, pp. 96–100, 2014.

[12] A. Khavasi, L. Chrostowski, Z. Lu, and R. Bojko, "Significant crosstalk reduction using all-dielectric CMOS-compatible metamaterials," *IEEE Photon. Technol. Lett.*, vol. 28, no. 24, pp. 2787–2790, Dec. 15, 2016.

[13] S. Jahani (2017). "*Photonic skin-depth engineering on a silicon chip using all-dielectric metamaterials*." [Online]. Available: https://arxiv.org/abs/1701.03093

[14] R. Halir, "Ultra-broadband nanophotonic beamsplitter using an anisotropic sub-wavelength metamaterial," *Laser Photon. Rev.*, vol. 10, no. 6, pp. 1039–1046, Nov. 2016.

[15] *GlobalFoundries: Technology Solutions/Silicon Photonics*. [Online]. Available: https://www.globalfoundries.com/technology-solutions/silicon-photonics

[16] B. Peng, C. Xiong, M. Khater, A. S. Jensen, W. M. J. Green, and T. Barwicz, "Metamaterial waveguides with low distributed backscattering in production O-band Si photonics," in *Proc. Opt. Fiber Conf.*, 2017, Paper Tu3K.3.

[17] J. D. Sarmiento-Merenguel, "Controlling leakage losses in subwavelength grating silicon metamaterial waveguides," *Opt. Lett.*, vol. 41, no. 15, pp. 3443–3446, 2016.

[18] A. Ortega-Moñux, "Disorder effects in subwavelength grating metamaterial waveguides," *Opt. Express*, vol. 25, no. 11, pp. 12222–12236, 2017.

[19] R. Halir, P. Cheben, D. Xu, J. H. Schmid, and S. Janz, "Colorless directional coupler with dispersion engineered sub-wavelength structure," *Opt. Express*, vol. 20, no. 12, pp. 13470–13477, 2012.

[20] Y. Wang, "Compact broadband directional couplers using subwavelength gratings," *IEEE Photon. J.*, vol. 8, no. 3, Jun. 2016, Art. no. 7101408.

[21] P. A. Besse, M. Bachmann, H. Melchior, L. B. Soldano, and M. K. Smit, "Optical bandwidth and fabrication tolerances of multimode interference couplers," *J. Lightw. Technol.*, vol. 12, no. 6, pp. 1004–1009, Jun. 1994.

[22] J. Xing, Z. Li, Y. Yu, and J. Yu, "Design of polarization-independent adiabatic splitters fabricated on silicon-on-insulator substrates," *Opt. Express*, vol. 21, no. 22, pp. 26729–26734, 2013.

[23] H. Yun, "Broadband 2×2 adiabatic 3 dB coupler using silicon-on-insulator sub-wavelength grating waveguides," *Opt. Lett.*, vol. 41, no. 13, pp. 3041–3044, 2016.

[24] L. Lu, "Inverse-designed single-step-etched colorless 3 dB couplers based on RIE-lag-insensitive PhC-like subwavelength structures," *Opt. Lett.*, vol. 41, no. 21, pp. 5051–5054, 2016.

[25] K. Xu, "Integrated photonic power divider with arbitrary power ratios," *Opt. Lett.*, vol. 42, no. 4, pp. 855–858, 2017.

[26] A. Densmore, "A silicon-on-insulator photonic wire based evanescent field sensor," *IEEE Photon. Technol. Lett.*, vol. 18, no. 23, pp. 2520–2522, Dec. 1, 2006.

[27] J. G. Wangüemert-Pérez, "Evanescent field waveguide sensing with subwavelength grating structures in silicon-on-insulator," *Opt. Lett.*, vol. 39, no. 15, pp. 4442–4445, 2014.

[28] V. Donzella, "Design and fabrication of SOI micro-ring resonators based on sub-wavelength grating waveguides," *Opt. Express*, vol. 23, no. 4, pp. 4791–4803, Feb. 2015.

[29] J. Flueckiger, "Sub-wavelength grating for enhanced ring resonator biosensor," *Opt. Express*, vol. 24, no. 14, pp. 15672–15686, 2016.

[30] H. Yan, "Unique surface sensing property and enhanced sensitivity in microring resonator biosensors based on subwavelength grating waveguides," *Opt. Express*, vol. 24, no. 26, pp. 29724–29733, 2016.

[31] L. Huang, "Improving the detection limit for on-chip photonic sensors based on subwavelength grating racetrack resonators," *Opt. Express*, vol. 25, no. 9, pp. 10527–10535, 2017.

[32] Z. Tu, D. Gao, M. Zhang, and D. Zhang, "High-sensitivity complex refractive index sensing based on Fano resonance in the subwavelength grating waveguide micro-ring resonator," *Opt. Express*, vol. 25, no. 17, pp. 20911–20922, 2017.

[33] Y. Xiong, J. G. Wangüemert-Pérez, D.-X. Xu, J. H. Schmid, P. Cheben, and W. N. Ye, "Polarization splitter and rotator with subwavelength grating for enhanced fabrication tolerance," *Opt. Lett.*, vol. 39, no. 24, pp. 6931–6934, 2014.

[34] L. Liu, Y. Ding, K. Yvind, and J. M. Hvam, "Silicon-on-insulator polarization splitting and rotating device for polarization diversity circuits," *Opt. Express*, vol. 19, no. 13, pp. 12646–12651, Jun. 2011.

[35] Y. Ding, L. Liu, C. Peucheret, and H. Ou, "Fabrication tolerant polarization splitter and rotator based on a tapered directional coupler," *Opt. Express*, vol. 20, no. 18, pp. 20021–20027, 2012.

[36] Y. Wang, "Ultra-compact sub-wavelength grating polarization splitter-rotator for silicon-on-insulator platform," *IEEE Photon. J.*, vol. 8, no. 6, Dec. 2016, Art. no. 7805709.

[37] Y. He, "Silicon polarization splitter and rotator using a subwavelength grating based directional coupler," in *Proc. Opt. Fiber Conf.*, 2017, Paper Th1G.6.

[38] L. Liu, Q. Deng, and Z. Zhou, "Manipulation of beat length and wavelength dependence of a polarization beam splitter using a subwavelength grating," *Opt. Lett.*, vol. 41, no. 21, pp. 5126–5129, 2016.

[39] Y. Xu and J. Xiao, "Compact and high extinction ratio polarization beam splitter using subwavelength grating couplers," *Opt. Lett.*, vol. 41, no. 4, pp. 773–776, 2016.

[40] Y. Xu and J. Xiao, "Ultracompact and high efficient silicon-based polarization splitter-rotator using a partially-etched subwavelength grating coupler," *Sci. Rep.*, vol. 6, no. 1, p. 27949, 2016.

[41] W. Jiang, X. Sun, and B. M. A. Rahman, "Compact and fabrication-tolerant polarization splitter based on horizontal triple-slot waveguide," *Appl. Opt.*, vol. 56, no. 8, pp. 2119–2126, Mar. 2017.

[42] S. Wu and J. Xiao, "Compact polarization rotator for silicon-based cross-slot waveguides using subwavelength gratings," *Appl. Opt.*, vol. 56, no. 17, pp. 4892–4898, 2017.

[43] Y. Xiong, D.-X. Xu, J. H. Schmid, P. Cheben, and W. N. Ye, "High extinction ratio and broadband silicon TE-pass polarizer using subwavelength grating index engineering," *IEEE Photon. J.*, vol. 7, no. 5, Oct. 2015, Art. no. 7802107.

[44] S. Chen, H. Wu, and D. Dai, "High extinction-ratio compact polarisation beam splitter on silicon," *Electron. Lett.*, vol. 52, no. 12, pp. 1043–1045, 2016.

[45] B. Shen, P. Wang, R. Polson, and R. Menon, "An integrated-nanophotonics polarization beamsplitter with $2.4 \times 2.4\ \mu m^2$ footprint," *Nature Photon.*, vol. 9, no. 6, pp. 378–382, 2015.

[46] A. Majumder, B. Shen, R. Polson, and R. Menon, "Ultra-compact polarization rotation in integrated silicon photonics using digital metamaterials," *Opt. Express*, vol. 25, no. 17, pp. 19721–19731, 2017.

[47] Z. Yu, H. Cui, and X. Sun, "Genetic-algorithm-optimized wideband on-chip polarization rotator with an ultrasmall footprint," *Opt. Lett.*, vol. 42, no. 16, pp. 3093–3096, 2017.

[48] G. Roelkens, D. Van Thourhout, and R. Baets, "High efficiency grating coupler between silicon-on-insulator waveguides and perfectly vertical optical fibers," *Opt. Lett.*, vol. 32, no. 11, pp. 1495–1497, 2007.

[49] X. Chen and H. K. Tsang, "Nanoholes grating couplers for coupling between silicon-on-insulator waveguides and optical fibers," *IEEE Photon. J.*, vol. 1, no. 3, pp. 184–190, Sep. 2009.

[50] R. Halir, "Continuously apodized fiber-to-chip surface grating coupler with refractive index engineered subwavelength structure," *Opt. Lett.*, vol. 35, no. 19, pp. 3243–3245, 2010.

[51] X. Xu, H. Subbaraman, J. Covey, D. Kwong, A. Hosseini, and R. T. Chen, "Colorless grating couplers realized by interleaving dispersion engineered subwavelength structures," *Opt. Lett.*, vol. 38, no. 18, pp. 3588–3591, 2013.

[52] L. Carroll, D. Gerace, I. Cristiani, and L. C. Andreani, "Optimizing polarization-diversity couplers for Si-photonics: Reaching the -1 dB coupling efficiency threshold," *Opt. Express*, vol. 22, no. 12, pp. 14769–14781, 2014.

[53] Y. Wang, "Focusing sub-wavelength grating couplers with low back reflections for rapid prototyping of silicon photonic circuits," *Opt. Express*, vol. 22, no. 17, pp. 20652–20662, 2014.

[54] D. Benedikovic, "High-efficiency single etch step apodized surface grating coupler using subwavelength structure," *Laser Photon. Rev.*, vol. 8, no. 6, pp. 93–97, 2014.

[55] D. Benedikovic, "Subwavelength index engineered surface grating coupler with sub-decibel efficiency for 220-nm silicon-on-insulator waveguides," *Opt. Express*, vol. 23, no. 17, pp. 22628–22635, 2015.

[56] D. Benedikovic, "Single-etch subwavelength engineered fiber-chip grating couplers for 1.3 μm datacom wavelength band," *Opt. Express*, vol. 24, no. 12, pp. 12893–12904, 2016.

[57] M. Fan, M. A. Popović, and F. X. Kärtner, "High directivity, vertical fiber-to-chip coupler with anisotropically radiating grating teeth," in *Proc. Conf. Lasers Electro-Optics (CLEO)*, 2007, Paper CTuDD3.

[58] M. T. Wade, "75% efficient wide bandwidth grating couplers in a 45 nm microelectronics CMOS process," in *Proc. IEEE Opt. Interconnects Conf. (OI)*, Apr. 2015, pp. 46–47.

[59] C. Alonso-Ramos, P. Cheben, A. Ortega-Moñux, J. H. Schmid, D.-X. Xu, and I. Molina-Fernández, "Fiber-chip grating coupler based on interleaved trenches with directionality exceeding 95%," *Opt. Lett.*, vol. 39, no. 18, pp. 5351–5354, Sep. 2014.

[60] D. Benedikovic, "High-directionality fiber-chip grating coupler with interleaved trenches and subwavelength index-matching structure," *Opt. Lett.*, vol. 40, no. 18, pp. 4190–4193, 2015.

[61] X. Chen, D. J. Thomson, L. Crudington, A. Z. Khokhar, and G. T. Reed, "Dual-etch apodised grating couplers for efficient fibre-chip coupling near 1310 nm wavelength," *Opt. Express*, vol. 25, no. 15, pp. 17864–17871, 2017.

[62] T. Watanabe, M. Ayata, U. Koch, Y. Fedoryshyn, and J. Leuthold, "Perpendicular grating coupler based on a blazed anti-back-reflection structure," *J. Lightw. Technol.*, vol. 35, no. 21, pp. 4663–4669, Nov. 1, 2017.

[63] D. Benedikovic, "L-shaped fiber-chip grating couplers with high directionality and low reflectivity fabricated with deep-UV lithography," *Opt. Lett.*, vol. 42, no. 17, pp. 3439–3442, Sep. 2017.

[64] L. Zhu, W. Yang, and C. Chang-Hasnain, "Very high efficiency optical coupler for silicon nanophotonic waveguide and single mode optical fiber," *Opt. Express*, vol. 25, no. 15, pp. 18462–18473, Jul. 2017.

[65] Q. Zhong, "Focusing-curved subwavelength grating couplers for ultra-broadband silicon photonics optical interfaces," *Opt. Express*, vol. 22,

no. 15, pp. 18224–18231, Jul. 2014.

[66] Y. Wang, *el al.*, "Design of broadband subwavelength grating couplers with low back reflection," *Opt. Lett.*, vol. 40, no. 20, pp. 4647–4650, Oct. 2015.

[67] A. Sánchez-Postigo, "Broadband fiber-chip zero-order surface grating coupler with 0.4 dB efficiency," *Opt. Lett.*, vol. 41, no. 13, pp. 3013–3016, 2016.

[68] M. Passoni, D. Gerace, L. Carroll, and L. C. Andreani, "Grating couplers in silicon-on-insulator: The role of photonic guided resonances on lineshape and bandwidth," *Appl. Phys. Lett.*, vol. 110, no. 4, p. 41107, 2017.

[69] J. Zou, Y. Yu, and X. Zhang, "Single step etched two dimensional grating coupler based on the SOI platform," *Opt. Express*, vol. 23, no. 25, pp. 32490–32495, 2015.

[70] J. Zou, Y. Yu, and X. Zhang, "Two-dimensional grating coupler with a low polarization dependent loss of 0.25 dB covering the C-band," *Opt. Lett.*, vol. 41, no. 18, pp. 4206–4209, Sep. 2016.

[71] J. Kang, "Focusing subwavelength grating coupler for mid-infrared suspended membrane germanium waveguides," *Opt. Lett.*, vol. 42, no. 11, pp. 2094–2097, 2017.

[72] T. Barwicz, "A metamaterial converter centered at 1490 nm for interfacing standard fibers to nanophotonic waveguides," in *Proc. Opt. Fiber Commun. Conf.*, 2016, Paper M2I.3.

[73] P. Cheben, D.-X. Xu, S. Janz, and A. Densmore, "Subwavelength waveguide grating for mode conversion and light coupling in integrated optics," *Opt. Express*, vol. 14, no. 11, pp. 4695–4702, 2006.

[74] P. Cheben, "Broadband polarization independent nanophotonic coupler for silicon waveguides with ultra-high efficiency," *Opt. Express*, vol. 23, no. 17, pp. 22553–22563, 2015.

[75] T. Barwicz, "An O-band metamaterial converter interfacing standard optical fibers to silicon nanophotonic waveguides," in *Proc. Opt. Fiber Commun. Conf.*, 2015, Paper Th3F.3.

[76] T. Barwicz, S. Kamlapurkar, Y. Martin, R. L. Bruce, and S. Engelmann, "A silicon metamaterial chip-to-chip coupler for photonic flip-chip applications," in *Proc. Opt. Fiber Commun. Conf.*, 2017, Paper Th2A.39.

[77] M. Papes, "Fiber-chip edge coupler with large mode size for silicon photonic wire waveguides," *Proc. SPIE*, vol. 9516, p. 95160K, May 2015.

[78] M.-J. Picard, Y. Painchaud, C. Latrasse, C. Larouche, F. Pelletier, and M. Poulin, "Novel spot-size converter for optical fiber to sub-μm silicon waveguide coupling with low loss, low wavelength dependence and high tolerance to alignment," in *Proc. Eur. Conf. Opt. Commun. (ECOC)*, 2015, pp. 1–3.

[79] Z. Wang, X. Xu, D. Fan, Y. Wang, and R. T. Chen, "High quality factor subwavelength grating waveguide micro-ring resonator based on trapezoidal silicon pillars," *Opt. Lett.*, vol. 41, no. 14, pp. 3375–3378, 2016.

[80] J. Wang, I. Glesk, and L. R. Chen, "Subwavelength grating Bragg grating filters in silicon-on-insulator," *Electron. Lett.*, vol. 51, no. 9, pp. 712–714, 2015.

[81] D. Pérez-Galacho, "Optical pump-rejection filter based on silicon sub-wavelength engineered photonic structures," *Opt. Lett.*, vol. 42, no. 8, pp. 1468–1471, 2017.

[82] J. Čtyroký *et al.*, "Design of narrowband Bragg spectral filters in subwavelength grating metamaterial waveguides," *Opt. Express*, vol. 26, no. 1, pp. 179–194, 2018.

[83] A. D. Simard and S. LaRochelle, "Complex apodized Bragg grating filters without circulators in silicon-on-insulator," *Opt. Express*, vol. 23, no. 13, pp. 16662–16675, 2015.

[84] B. Naghdi and L. R. Chen, "Silicon photonic contradirectional couplers using subwavelength grating waveguides," *Opt. Express*, vol. 24, no. 20, pp. 23429–23438, 2016.

[85] B. Liu, "Silicon photonic bandpass filter based on apodized subwavelength grating with high suppression ratio and short coupling length," *Opt. Express*, vol. 25, no. 10, pp. 11359–11364, 2017.

[86] B. Naghdi and L. R. Chen, "Spectral engineering of subwavelength- grating-based contradirectional couplers," *Opt. Express*, vol. 25, no. 21, pp. 25310–25317, 2017.

[87] A. Y. Piggott, J. Lu, K. G. Lagoudakis, J. Petykiewicz, T. M. Babinec, and J. Vučković, "Inverse design and demonstration of a compact and broadband on-chip wavelength demultiplexer," *Nature Photon.*, vol. 9, no. 6, pp. 374–377, 2015.

[88] L. Liu, Q. Deng, and Z. Zhou, "An ultra-compact wavelength diplexer engineered by subwavelength grating," *IEEE Photon. Technol. Lett.*, vol. 29, no. 22, pp. 1927–1930, Nov. 15, 2017.

[89] A. Ortega-Moñux, "An ultra-compact multimode interference coupler with a subwavelength grating slot," *Laser Photon. Rev.*, vol. 7, no. 2, pp. L12–L15, 2013.

[90] J. S. Penadés, "Suspended silicon mid-infrared waveguide devices with subwavelength grating metamaterial cladding," *Opt. Express*, vol. 24, no. 20, pp. 22908–22916, 2016.

[91] J. Penadés, "Suspended silicon waveguides for long-wave infrared wavelengths," *Opt. Lett.*, vol. 43, no. 4, pp. 795–798, 2018.

[92] W. Zhou, Z. Cheng, X. Wu, B. Zhu, X. Sun, and H. K. Tsang, "Fully suspended slot waveguides for high refractive index sensitivity," *Opt. Lett.*, vol. 42, no. 7, pp. 1245–1248, 2017.

[93] W. Zhou, Z. Cheng, X. Wu, B. Zheng, X. Sun, and H. K. Tsang, "Fully suspended mid-infrared racetrack resonator with subwavelength grating cladding," in *Proc. IEEE 14th Int. Conf. Group IV Photon. (GFP)*, Aug. 2017, pp. 93–94.

[94] J. Xiao and Y. Xu, "Ultracompact and broadband silicon-based strip-to-slot mode converter," *IEEE Photon. Technol. Lett.*, vol. 28, no. 13, pp. 1414–1417, Jul. 1, 2016.

[95] J. Wang, "Subwavelength grating enabled on-chip ultra-compact optical true time delay line," *Sci. Rep.*, vol. 6, Jul. 2016, Art. no. 30235.

[96] P. J. Bock, "Subwavelength grating Fourier-transform interferometer array in silicon-on-insulator," *Laser Photon. Rev.*, vol. 7, no. 6, pp. L1–L4, 2013.

[97] Z. Ruan, L. Shen, S. Zheng, and J. Wang, "Subwavelength grating slot (SWGS) waveguide on silicon platform," *Opt. Express*, vol. 25, no. 15, pp. 18250–18264, 2017.

[98] G. Gao, "Transmission of 2.86 Tb/s data stream in silicon subwavelength grating waveguides," *Opt. Express*, vol. 25, no. 3, pp. 2918–2927, 2017.

[99] L. H. Gabrielli, D. Liu, S. G. Johnson, and M. Lipson, "On-chip transformation optics for multimode waveguide bends," *Nature Commun.*, vol. 3, Nov. 2012, Art. no. 1217.

[100] J. Zhang and S. He, "Cladding-free efficiently tunable nanobeam cavity with nanotentacles," *Opt. Express*, vol. 25, no. 11, pp. 12541–12551, 2017.

[101] Z. Jafari and A. Zarifkar, "Fabrication-friendly subwavelength-structure-assisted waveguide for dispersion engineering," *Appl. Opt.*, vol. 55, no. 32, pp. 9084–9090, 2016.

[102] Z. Jafari and A. Zarifkar, "Dispersion flattened single etch-step waveguide based on subwavelength grating," *Opt. Commun.*, vol. 393, pp. 219–223, Jan. 2017.

[103] D. Benedikovic, "Dispersion control of silicon nanophotonic waveguides using sub-wavelength grating metamaterials in near- and mid-IR wavelengths," *Opt. Express*, vol. 25, no. 16, pp. 19468–19478, 2017.

[104] Z. Jafari, A. Zarifkar, and M. Miri, "Compact fabrication-tolerant subwavelength-grating-based two-mode division (de)multiplexer," *Appl. Opt.*, vol. 56, no. 26, pp. 7311–7319, 2017.

[105] D. González-Andrade, "Ultra-broadband mode converter and multiplexer based on sub-wavelength structures," *IEEE Photon. J.*, vol. 10, no. 2, Apr. 2018, Art. no. 2201010.

ABOUT THE AUTHORS

Robert Halir received the M.Sc. degree in telecommunications engineering with first-class honors and the Ph.D. degree from Málaga University, Málaga, Spain, in 2006 and 2010, respectively.

Currently, he is an Assistant Professor at Málaga University, as well as a Researcher at the Andalusian Institute for Nano-medicine and Biotechnology (Bionand). He has coauthored more than 60 papers in the field of integrated optics and holds several patents. His research currently focuses on high performance silicon photonic devices, highly efficient fiber-to-chip couplers and photonic biosensors.

Alejandro Ortega-Moñux received the M.Sc. degree in telecommunications engineering and the Ph.D. degree from Málaga University, Málaga, Spain, in 1998 and 2008, respectively.

Since 1999, he has been with the ETSI Telecomunicación, Universidad de Málaga, as an Assistant and then Associate Professor. He is coauthor of more than 50 journal and conference papers and holds several patents. His research interest is in the area of the modeling and design of photonic integrated circuits, such as multimode interference couplers, fiber-to-chip grating couplers, polarization beam splitters/rotators and subwavelength periodic structures.

Daniel Benedikovic received the M.Sc. degree in telecommunications and the Ph.D. degree from the University of Žilina, Žilina, Slovakia, in 2011 and 2015, respectively.

During his study, he completed several educational and scientific internships in Finland at Aalto University, in Spain at the University of Málaga, and in Canada at the National Research Council. In 2015, he joined the Centre de Nanoscience et de Nanotechnology, CNRS, Université Paris-Sud, Université Paris-Saclay in France, working as a post-doc Researcher. His current research activity mainly involves the development, design, and optical characterization of active and passive silicon photonic components and sub-wavelength grating nanostructures.

Goran Z. Mashanovich received the Dipl. Ing. and M.Sc. degrees in optoelectronics from the Faculty of Electrical Engineering, University of Belgrade, Belgrade, Serbia, and the Ph.D. degree in silicon photonics from the University of Surrey, Guildford, U.K.

He is a Professor of Group IV Photonics at the Optoelectronics Research Centre, University of Southampton, Southampton, U.K. His research interests include near- and mid-IR silicon and germanium photonic circuits. He is a coauthor of more than 300 publications in the field and a member of several international conference committees related to photonics.

J. Gonzalo Wangüemert-Pérez was born in Canary Islands, Spain. He received the M.Sc. degree in telecommunications engineering from the Polytechnic University of Madrid, Madrid, Spain, in 1992, and the Ph.D. degree from the University of Málaga, Málaga, Spain, in 1999.

In 1993, he joined the University of Málaga, first as Assistant Professor, next as Associate Professor, and then as Full Professor. His research activity has mainly been focused on the field of integrated optics, including the following topics of interest: development and validation of CAD-tools for modeling and simulation of integrated optical devices and analysis and design of integrated optical devices for applications in communications and biosensing. He has authored or coauthored more than 40 journal papers and 100 conference papers.

Jens H. Schmid received the Ph.D. degree from the University of British Columbia, Vancouver, BC, Canada, in 2004, for his work on *in situ* etching and molecular beam epitaxial regrowth on III-V semiconductors.

After working for a year as a Research Scientist for VSM MedTech, a medical device company in Coquitlam, BC, Canada, where he developed fabrication processes for superconducting quantum interference devices, he joined the nanofabrication group at the National Research Council Canada (NRC) in 2005. He is currently a Senior Research Officer with the Advanced Electronics and Photonics Research Centre of NRC and also an Adjunct Professor with the Department of Electronics at Carleton University. His current research interests are the fabrication, design, characterization and simulation of silicon photonic devices and nanostructures.

Íñigo Molina-Fernández received the Ingeniero de Telecomunicación degree from the Universidad Politécnica de Madrid, Madrid, Spain, in 1989, and the Ph.D. degree from the Universidad de Málaga, Málaga, Spain, in 1993.

Since 1989, he has been with the ETSI Telecomunicación, Universidad de Málaga, as an Associate and then Full Professor, where he is the leader of the Photonics and RF group. His research interest is in the area of optical and microwave communications where he has led several projects regarding design of optical integrated devices and prototyping of microwave/millimeter wave systems. He is coauthor of more than 100 international publications in microwave and photonic topics. He has been participating in more than 25 research and development national and international projects.

Pavel Cheben is a Principal Research Officer at the National Research Council (NRC) of Canada. He is also an Honorary Professor at the University of Malaga and Adjunct Professor at Carleton University, McMaster University, University of Ottawa, and University of Zilina. He was one of the Lead Scientists starting up Optenia, Inc., and developed the first commercial echelle-grating WDM multiplexer. Before joining the NRC, he was with the National Institute for Aerospace Technology of the Ministry of Defense, Spain. His research focusses on silicon photonics, subwavelength metamaterial nanophotonic structures, and on-chip spectrometers and biosensors. He has coauthored more than 400 journal and conference papers, has 30 patent applications and over 180 invited presentations. Since 2011, he has been the most published scientist at the NRC of Canada.

Dr. Cheben is an elected Fellow of the European Optical Society, of the Optical Society of America and of the Institute of Physics.